## Odyssey Rapid #: -6793870 utah.illiad.oclc.org/UUM

CALL #: <a href="http://rlib.pace.edu/login?">http://rlib.pace.edu/login?</a>

url=http://search.proquest.com/pu ...

**LOCATION:** VZP :: Electronic Journals :: Science Journals

TYPE: Article CC:CCL

JOURNAL TITLE: Proceedings of the Institution of Mechanical Engineers. Part F, Journal of rail and

rapid transit

USER JOURNAL Proceedings of the Institution of Mechanical Engineers. Part F, Journal of rail and

TITLE: rapid transit

VZP CATALOG Proceedings of the Institution of Mechanical Engineers. Part F, Journal of rail and

TITLE: rapid transit

ARTICLE TITLE: Stress changes in the ground below ballasted railway track during train passage.

ARTICLE AUTHOR: W Powrie, L A Yang and C R I Clayton

VOLUME: 221
ISSUE: 2
MONTH: MARCH
YEAR: 2007
PAGES: 247-262
ISSN: 0954-4097

OCLC #:

CROSS REFERENCE [TN:1018363][ODYSSEY:utah.illiad.oclc.org/UUM]

ID:

VERIFIED:

**BORROWER:** UUM :: Marriott Library

**PATRON:** 



This material may be protected by copyright law (Title 17 U.S. Code)  $6/24/2013\ 2:48:02\ PM$ 

### Stress changes in the ground below ballasted railway track during train passage

Powrie, W; Yang, L A; Clayton, C R I

Proceedings of the Institution of Mechanical Engineers; Jun 2007; 221, F2; ProQuest Central

247

# Stress changes in the ground below ballasted railway track during train passage

W Powrie, L A Yang\*, and C R I Clayton

Rail Research UK/Southampton Railway Systems Research (SR2), University of Southampton, Southampton, UK

The manuscript was received on 23 June 2006 and was accepted after revision for publication on 1 February 2007.

DOI: 10.1243/0954409JRRT95

**Abstract:** The design of railway track formations has traditionally been empirically rather than analytically based, with ballast and sub-ballast layer thicknesses specified mainly on the basis of previous practice. Recent design methods are more scientifically based, and for the most advanced design methods currently in use, input parameters are typically determined from cyclic triaxial testing.

The changes in stress experienced by an element of soil below a railway track as a train passes are complex, involving (for example) a cyclic rotation of the principal stress directions. In these conditions, soil element testing in uniaxial compression may lead to the underestimation of vertical strains. Testing in a hollow cylinder apparatus, which can impose the rotations in principal stress direction likely to be experienced by a soil element in the field, may therefore be preferable to triaxial testing. However, there are as yet no data to guide the designer to a rational specification of a testing programme in this more complex apparatus.

This article reports the results of finite element analyses carried out to investigate the stress changes experienced by an element of soil beneath a ballasted railway track during train passage. The effects of element location, the initial *in situ* stress state of the soil, and the elastic parameters used to characterize its behaviour are investigated, and the modelling of the stress paths in a cyclic hollow cylinder apparatus is discussed.

**Keywords:** principal stress rotation, railway track, numerical modelling and analysis, hollow cylinder apparatus

### 1 INTRODUCTION

One of the aims of the ballast and sub-ballast layers below a traditional railway track is to reduce the stresses transmitted to the subgrade to values that will not cause excessive (plastic) deformation or failure. However, the design of railway tracks has traditionally been empirically rather than analytically based, with ballast and sub-ballast layer thicknesses specified on the basis of previous practice, almost irrespective of the nature or condition of the subgrade. Even where the ballast and sub-ballast layer thicknesses are

determined more analytically [1, 2], stresses at the top of the subgrade are often calculated using equations that are either empirical or based on the Boussinesq solution for the vertical stresses in an infinite elastic half space [3].

For example, the American Railway Engineering Association manual [1] assumes an allowable subgrade bearing pressure of 138 kPa for all subsoil conditions. Recognizing that this value may be too conservative for some soils and too large for softer deposits, Raymond [2] modified the original AREA method by using Casagrande's soil classification [4] as an indication of soil strength. British Rail [5] developed an approach based on limiting the stress transmitted to the subgrade to a 'threshold stress', determined from cyclic triaxial compression tests, such that excessive plastic deformation will not occur during the lifetime of the track as defined by a number of applications of a given axle load.

Proc. IMechE Vol. 221 Part F: J. Rail and Rapid Transit

<sup>\*</sup>Corresponding author: School of Civil Engineering and the Environment, Rail Research UK, University of Southampton, Highfield, Southampton, Hampshire SO17 1BJ, UK. email: liang@soton.ac.uk

The threshold stress method and the methods proposed by Li and Selig [6,7] are more scientifically based. The stress in the subgrade is calculated on an essentially static basis, with the ballast, sub-ballast, and subsoil treated as layered elastic materials. However, in the cyclic triaxial tests used to determine the threshold stress [5], cumulative plastic strain [8], and strength and stiffness [9], only the major (axial) principal stress is cycled [10]. In reality, the changes in stress within an element of soil below a railway track are quite complex and involve a rotation of the principal stress directions as a train passes (Fig. 1) [11, 12]. In these conditions, testing in uniaxial compression may under-estimate both individual (i.e. within a cycle) and cumulative axial (vertical) strains (Fig. 2) [13].

In addition to rotating in the longitudinal plane as indicated in Fig. 1, the principal stresses will also (except on the centre-line of the track) rotate in the transverse plane. The magnitude of the stress cycle will decrease with depth as the loads spread through the soil; especially relative to the in situ or confining stress, which increases with depth. The number of cycles will also decrease with depth, as the effects of individual axles and then bogie pairs merge. Thus, near the surface, the magnitude of the stress cycle is the greatest, the confining stress is the smallest, and the number of cycles is the largest as the effects of individual axles are felt. At depth, the magnitude of the stress cycle is smaller, the confining stress is greater, and the number of cycles is reduced as only the effect of the train may be felt.

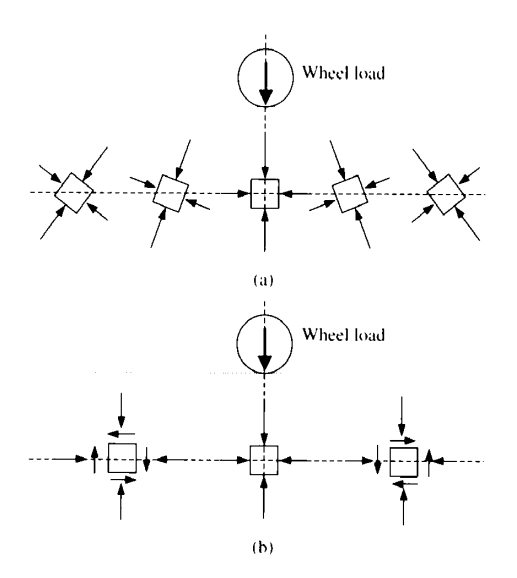


Fig. 1 Stresses on pavement elements: (a) principal stresses and planes; (b) shear and normal stresses on horizontal and vertical planes (from reference [11])

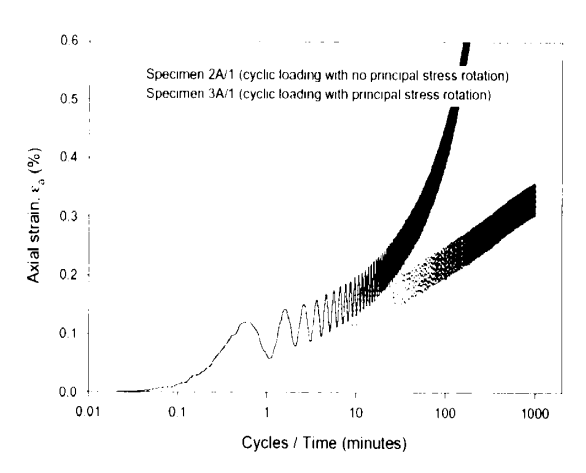


Fig. 2 Importance of principal stress rotation on cumulative plastic strains in a soil element test (redrawn from reference [13])

In laboratory investigations of the response of soil elements to the real nature of the cyclic loads associated with the passage of trains, it is necessary to have a clear understanding of both the magnitude and number of loading cycles and the degree of principal stress rotation (PSR) (about both transverse and longitudinal axes). This article investigates the variation of these loading parameters with depth, by means of finite element analysis (FEA). Guidelines for appropriate laboratory element testing in connection with a stress-based design are also presented.

### 2 FEA: INITIAL CONSIDERATIONS

In setting up the finite element analyses, a number of factors were considered, including the need to model a typical track system geometry, loading, the adequacy of a static analysis, the soil model, mesh boundary positions, and the level of discretization required. Initial analyses were developed in two dimensions before carrying out full three-dimensional analyses, using the finite element package ABAQUS/STANDARD version 6.5 in both cases [14]. A two-dimensional model requires relatively little computational time and memory and was suitable for validation of the general approach, including identifying the mesh size and level of discretization required. However, it cannot accurately reproduce the three-dimensional nature of actual traffic loadings, for which a three-dimensional model was developed.

In presenting the results, lengths are normalized with respect to the sleeper length S (=2420 mm), and stresses with respect to a nominal maximum surface stress between sleeper and ballast  $\sigma_{\rm sb}$  (=the axle load divided by the plan area of the sleeper).

Proc. IMechE Vol. 221 Part F: J. Rail and Rapid Transit

### 2.1 Track system geometry

In a traditional railway track system, the steel rails are supported on timber or reinforced concrete sleepers typically spaced at 650 mm centres. The sleepers are embedded into a layer of coarse granular aggregate (ballast), below which an engineered sub-ballast layer may be placed, although this is rare in the UK except on modern high-speed lines. In upgrade work (e.g. the UK West Coast Main Line), a geotextile layer might be placed over a prepared subgrade layer (traditionally called a sand blanket in the UK) to act as a separator to prevent the migration of ballast or sub-ballast particles [15, 16].

The typical track structure shown in Fig. 3 was modelled in the FEA, but without the geotextile. Following the International Union of Railways (UIC) Code 719R [16] and practice on the UK Channel Tunnel Rail Link [17], depths of 300 mm of ballast, 200 mm of sub-ballast, and 500 mm of prepared subgrade were adopted in the analysis. The rail crosssection was modelled as a rectangle of 153 mm high  $\times$ 78 mm wide. With a Young's modulus  $E = 210 \,\text{GPa}$ , the bending stiffness  $EI = 4889 \text{ kN m}^2$  corresponds to a 56.4-kg/m steel rail to BS113A [15]. Sleepers were modelled as cuboids of 200 mm high, 242 mm wide, and 2420 mm long, with a spacing of 650 mm between centres. Rail pads were not modelled explicitly, as they would have no effect on the transmission of loads to the ground in a static analysis.

### 2.2 Loads applied

The analyses were based on a typical modern freight car-an MBA box wagon as used by English Welsh

& Scottish Railways (EWS) to convey heavy bulk materials such as coal, aggregates, and construction materials. These have an axle load of 25.4 tonnes (the maximum normally permitted on the UK rail network), corresponding to a static wheel load of 125 kN.

In addition to vertical loads, a moving train will exert horizontal or shear loads at the wheel–rail interface. For a train travelling at a constant speed, forward forces will be required to overcome the effects of rolling and wind resistance. These will, however, generally be small: Esveld [18] suggests a maximum of 0.2 per cent of the static vertical wheel load. Forces applied when the train is accelerating or braking will generally be rather greater. Perhaps the largest horizontal forces will be associated with the acceleration of a locomotive-hauled train (rather than a trainset with distributed traction motors), because a sufficient force to accelerate the whole train must be applied at the wheels of the locomotive alone.

A Class 66 locomotive exerting its maximum tractive effort will apply a horizontal wheel force of 34.1 kN or 32 per cent of the static vertical wheel load of 105 kN. The theoretical maximum braking capacity is equivalent to a horizontal wheel load of 57 kN or 54 per cent of the static vertical load, although, in reality, this might be limited by the coefficient of sliding friction of dry steel on dry steel of 0.4 [19]. For the purpose of analysis, the maximum horizontal force is often taken as 25 per cent of the vertical static load [18]. When a horizontal acceleration or braking load of this magnitude was applied in the FEA, the maximum differences in stress were 17 per cent in  $\sigma_{xx}$ , 6 per cent in  $\sigma_{yy}$  and  $\sigma_{zz}$ , and 5 per cent in  $\tau_{xz}$  (compared with the analysis in which only the vertical static load was

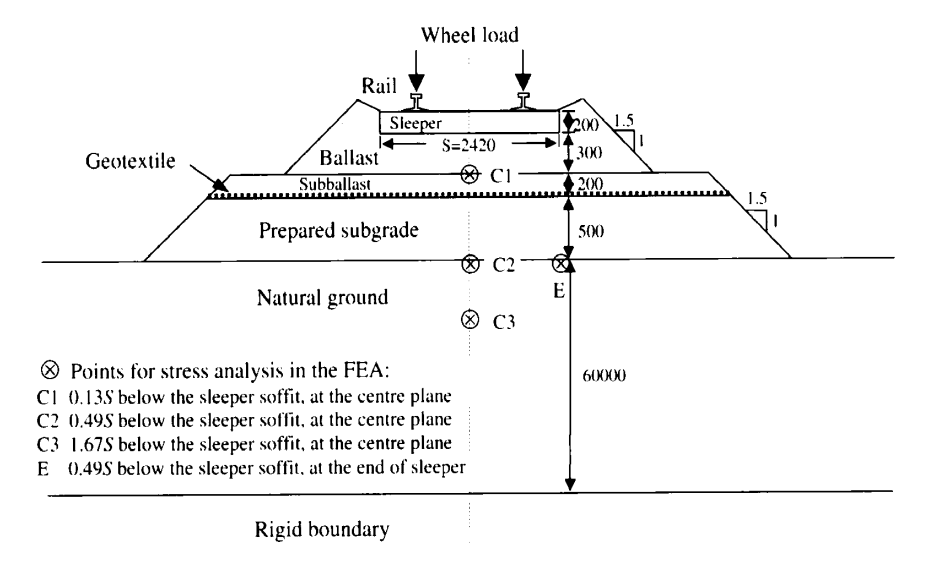


Fig. 3 Schematic cross-section of a typical track structure (dimensions in mm)

Proc. IMechE Vol. 221 Part F: J. Rail and Rapid Transit

applied) at the ballast surface; 14 per cent in  $\sigma_{xx}$  and 6 per cent in  $\tau_{xz}$  at the surface of sub-ballast; and 4.5 per cent in  $\sigma_{xx}$  and 9 per cent in  $\tau_{xz}$  at the soil surface. However, the pattern of major PSR was not affected. Thus, the effect on PSR of directly applied shear loads is small compared with the effect of the horizontal distance from the vertical load and may reasonably be neglected.

### 2.3 Adequacy of a static analysis

In reality, vertical loads exerted by a moving railway vehicle may be greater or less than the static value, depending on whether the vehicle is momentarily accelerating downward or upward. However, it is a common practice to carry out a static analysis, in which dynamic effects are taken into account by multiplying the static load by a dynamic amplification factor (DAF). The DAF depends on the train speed, the track quality, and confidence intervals required and may normally range from 1.1 to 2.8 [18]. DAFs have not been used in this analysis, but with the geomaterials assumed to behave as linear elastic materials, the calculated stress changes will be directly proportional to the loads. Dynamic finite element analyses carried out by Grabe [12] indicated that, for speeds up to 240 km/h, the impact of dynamic effects on the calculated maximum changes in stress in the ground below a railway line were small, whereas the ground response from moving train loads is essentially quasistatic for speeds up to 140 km/h [20]. Thus, it was considered that, for the purpose of determining representative stress changes for laboratory testing, a static analysis would suffice.

### 2.4 Soil models

The geotechnical materials were modelled as linear elastic using the parameters indicated in Table 1, except where otherwise stated. Most of the analyses were carried out with Poisson's ratio  $\nu$  for the natural ground set to a value  $\nu_u$  ( $\sim 0.5$  for an isotropic soil) consistent with deformations at constant volume, and should therefore be interpreted in terms

of total stresses. Some isotropic analyses were carried out with Poisson's ratios  $\nu'$  of 0.3 and 0.1; the Young's modulus in these cases was multiplied by  $(1+\nu')/(1+\nu_u)$  to give the same shear modulus G. With a reduced Poisson's ratio, volume change will occur: these analyses therefore represent a partly saturated material, in which volume changes may occur without any overall loss of pore water.

In most of the analyses, the Young's modulus E of the natural ground was assumed to increase linearly with depth  $\lfloor 21 \rfloor$ 

$$E = E_0 + m \cdot z \tag{1}$$

with  $E_0 = 30 \text{ MPa}$  and m = 4.5 MPa/m, typical of undrained parameters for the stiff, overconsolidated London Clay [22].

### 2.5 Two-dimensional analyses to investigate mesh size and level of discretization required

Initial plane strain (two-dimensional) finite element analyses were carried out on a cross-section of the track using 8-node biquadratic elements with reduced integration to determine a suitable mesh size and density and to validate the approach with reference to standard, closed-form solutions for a total stress analysis with soil deformation at constant volume ( $v \sim$ 0.5). Attention was focused on the stresses induced by train loading; hence stresses arising from the selfweight of all materials were ignored. Because in a two-dimensional analysis the sleepers are inherently continuous, the Young's modulus of the sleepers was scaled by the ratio of sleeper width w to spacing a to give the same value of lateral bending stiffness EI per metre run of the track as for the discrete sleepers in reality

$$E(2D) = \frac{E(3D) \times w}{a} = \frac{34 \text{ GPa} \times 242 \text{ mm}}{650 \text{ mm}} = 13 \text{ GPa}$$
(2)

A wheel load of 125 kN was applied to the rail, as described above.

Table 1 Material properties used in finite element analyses

Component description	Young's modulus (MPa)	Poisson's ratio	Unit weight (kN/m³)	Remarks
Rail	210 000	0.3	76.93	Cross-section 78 mm wide × 153 mm deep
Sleeper	34 000	0.3	23.52	Cross-section 242 mm wide × 200 mm deer
Ballast	310	0.3	16.66	
Sub-ballast	130	0.49	22.54	
Prepared subgrade	100	0.49	19.6	
Natural ground	30	0.49	19.6	For Gibson soil, $E = 30 + mz$ , $m = 4.5$

Proc. IMechE Vol. 221 Part F: J. Rail and Rapid Transit

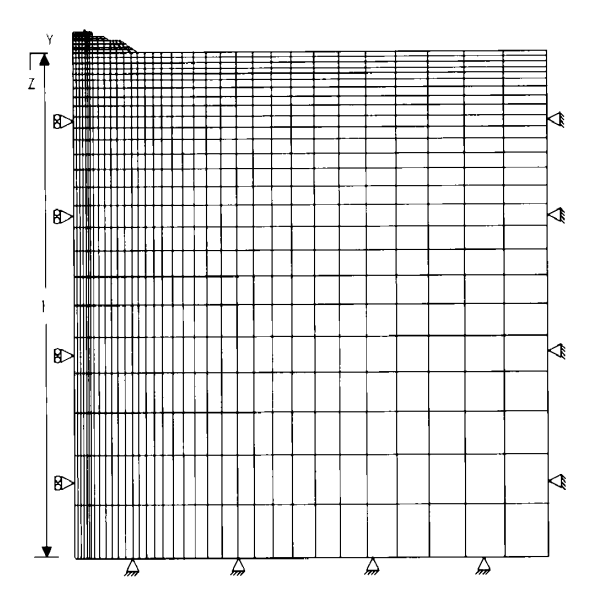


Fig. 4 Two-dimensional finite element mesh – intermediate density

Three mesh densities were investigated. The intermediate mesh, which comprised 1634 elements (Fig. 4): the coarse mesh had half the element density (i.e. approximately one-quarter of the number of elements) and the fine mesh had twice the element density (i.e. about four times the number of elements). In all the cases, the bottom and right-hand boundaries were restrained (pinned) in both the horizontal and vertical directions. The left-hand boundary was prevented from moving in the horizontal direction, but free to move vertically. All three meshes gave almost identical ground-surface displacements. However, differences in stress were calculated within the ballast layer, particularly for the coarse mesh

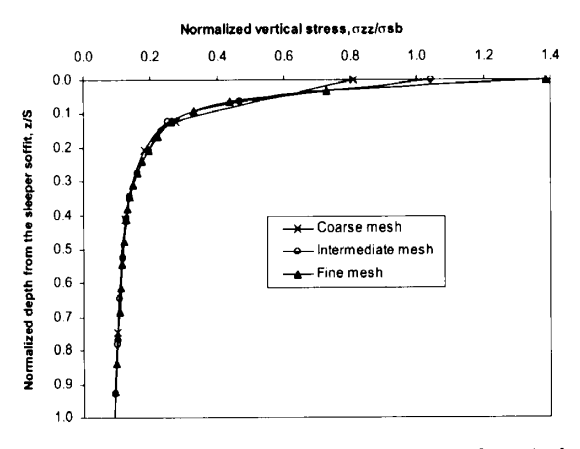


Fig. 5 Mesh convergence study-variation of vertical stress with depth below the end of the sleeper for different mesh densities

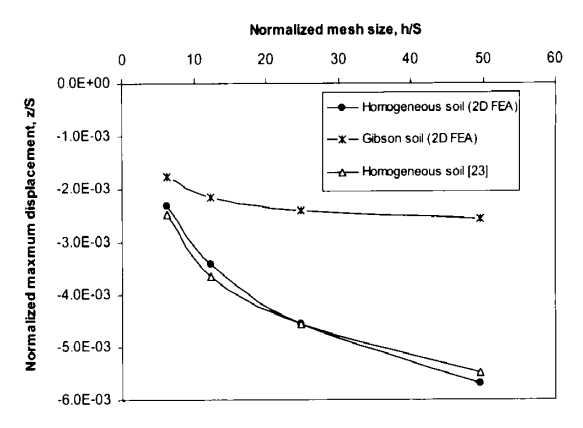


Fig. 6 Maximum displacement at the ground surface for different mesh sizes

(Fig. 5). The intermediate mesh was therefore used for subsequent two-dimensional analyses.

Four mesh sizes were investigated, of dimensions  $15 \text{ m} \times 15 \text{ m}$ ,  $30 \text{ m} \times 30 \text{ m}$ ,  $60 \text{ m} \times 60 \text{ m}$ , and  $120\,\text{m} \times 120\,\text{m}$  (depth and width of natural ground), comprising 614, 944, 1634, and 3614 elements, respectively. The maximum displacements at ground level are plotted against the mesh size in Fig. 6 for both a Gibson soil ( $E = 30 + 10.89 \cdot (z/S)$  MPa) and a homogeneous soil with a uniform Young's modulus E =30 MPa. For the analyses using the Gibson soil, the maximum surface displacement converged rapidly and a mesh size of  $60 \text{ m} \times 60 \text{ m}$  (i.e.  $24.8S \times 24.8S$ ) was sufficient (Fig. 7, which shows the variation with depth of the vertical stresses on the centre-line of each mesh, confirms this). For the homogeneous soil, the maximum surface displacement continued to increase with mesh depth, even for the larger meshes. However, this is to be expected as it agrees with the closed-form elastic solution [23], in which the surface settlement increases with the depth of the half space.

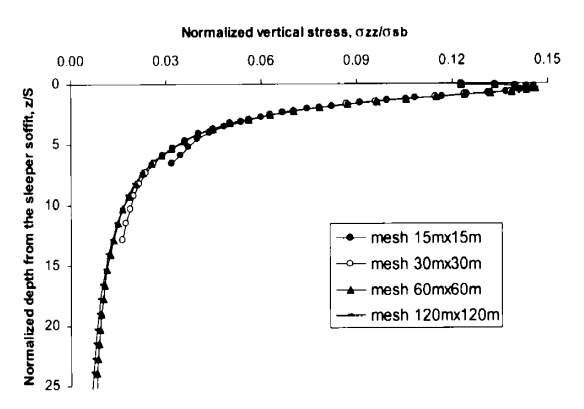


Fig. 7 Variation in vertical stress with depth on the centre-line for different mesh sizes for Gibson soil

Proc. IMechE Vol. 221 Part F: J. Rail and Rapid Transit

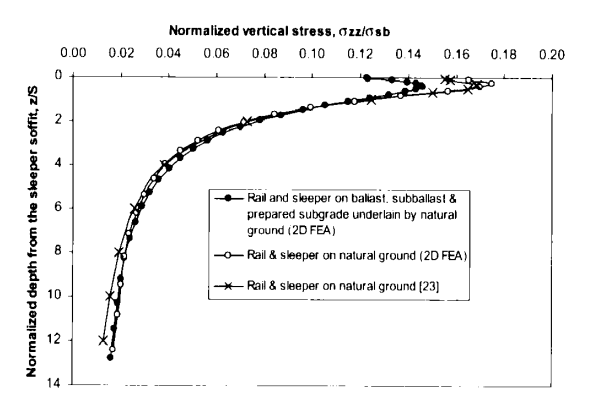


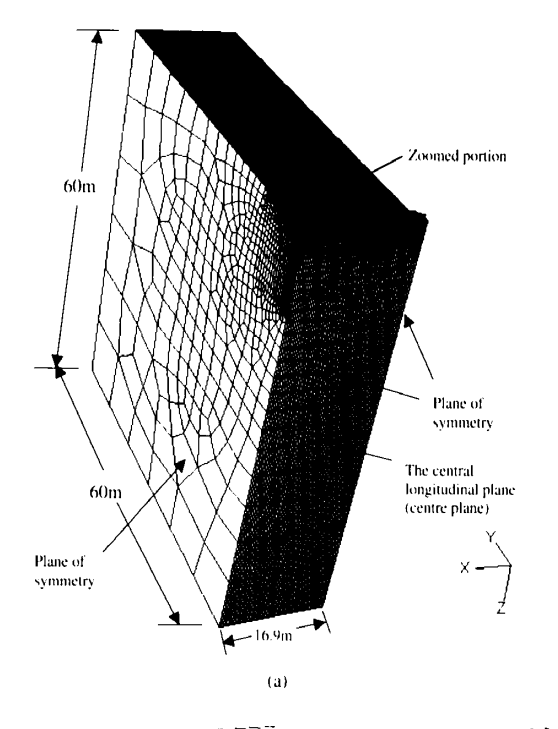
Fig. 8 Variation in vertical stress with depth on the centre-line, illustrating the function of the ballast, sub-ballast, and prepared subgrade layers for Gibson soil

One of the important functions of the ballast, sub-ballast and prepared subgrade is to reduce the traffic-induced stresses to levels that will not cause excessive plastic deformation or failure of the subgrade [3]. Figure 8 shows that, for the track system geometry investigated, the stress at the top of natural ground would increase by about 20 per cent if the sleepers were laid directly on it.

### 3 THREE-DIMENSIONAL ANALYSES

The three-dimensional mesh is shown in Fig. 9; materials properties were again as given in Table 1. The analyses made full use of the symmetry by modelling one-half of the track (i.e. half a sleeper and one rail) as viewed in cross-section, and the distance between the centres of successive vehicles in what is effectively an infinitely long train. A total of 50 782 20-noded quadratic brick elements with reduced integration were used.

The length of the mesh in the longitudinal (x) direction was taken as that of an MBA box wagon (Fig. 10). In the vertical (z) and transverse (y) directions, the dimensions of the mesh were set at 60 m: the results of the two-dimensional analyses (which are more onerous in this respect) indicated that this should be sufficient to eliminate the boundary effects. Smaller elements were used near the track where the changes of stresses and strains were expected to be the greatest. The bottom and far-lateral (normal to the z and y planes respectively) boundaries were prevented from movement (i.e. pinned) in all three directions. The longitudinal boundaries (normal to the x direction) were restrained in the x direction only, but otherwise free to move. The centre plane was restrained in the y direction only.



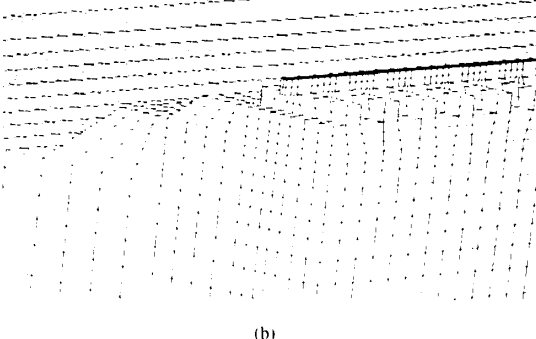


**Fig. 9** (a) Three-dimensional finite element mesh and (b) zoomed portion

Four wheel loads of 125 kN each were applied on the rail, in the positions corresponding to the axles on the bogies at each end of a pair of adjoining wagons as indicated in Fig. 10. In the absence of dynamic interactions between the vehicle and the track, the stresses caused by a continuously moving load on a soil element below a railway track may be determined by considering a succession of soil elements in different locations relative to a static load. Figure 11 shows that the difference between a wheel load being applied exactly on or mid-way between sleepers is negligible at depths greater than 0.3S below the sleeper soffit. The maximum vertical stress is about  $0.1\sigma_{\rm sb}$  at 0.1Sand  $0.05\sigma_{\rm sh}$  at 0.3S, which is consistent with the results of a GEOTRACK model (see Fig. 5.13 and Fig. 5.14 in reference [3]).

Proc. IMechE Vol. 221 Part F: J. Rail and Rapid Transit

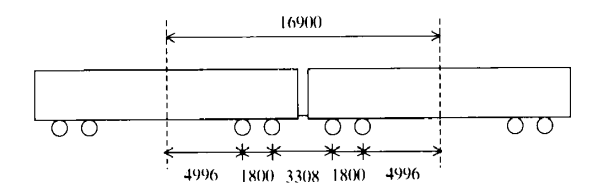


Fig. 10 Wheel load configuration and axes of symmetry used in the three-dimensional finite element analyses (based on an EWS MBA box wagon; dimensions in mm)

As before, the results presented initially relate only to the incremental stresses due to the wheel loads applied and do not include the *in situ* stresses. However, the initial stress state is important in considering the absolute directions and hence rotations of the principal stresses during loading and will be discussed later.

It is generally accepted that the calculated changes in vertical stress within a body of soil idealized as a uniform elastic half space due to the application of a pattern of surface loads are relatively insensitive to the elastic parameters assumed. However, the same is not true for strains and possibly other stress components, which may vary significantly with heterogeneity and anisotropy [23, 24].

### 3.1 Homogeneous, isotropic analyses without initial stresses

Analyses were carried out for a homogeneous, isotropic soil deforming at constant volume ( $\nu = \nu_u \approx 0.49$ ) with (undrained) Young's moduli of 30, 60, and 90 MPa. The results of these analyses, plotted as the inclination of the major principal stress increment to the vertical against the distance from the centre of the first box wagon, are summarized in Fig. 12 for depths of 0.49S and 1.67S below the sleeper soffit.

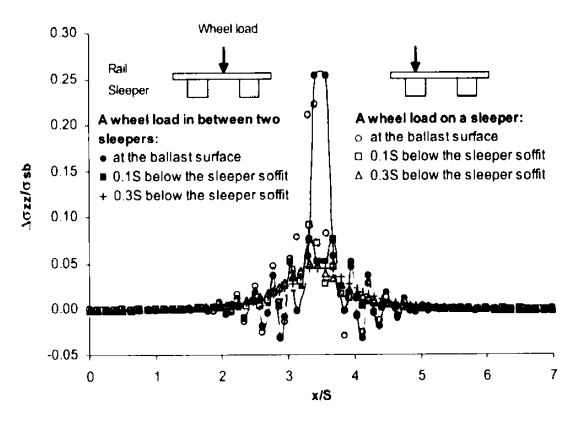
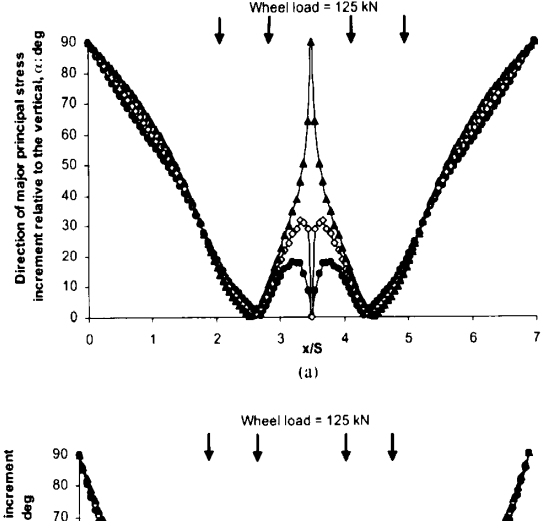
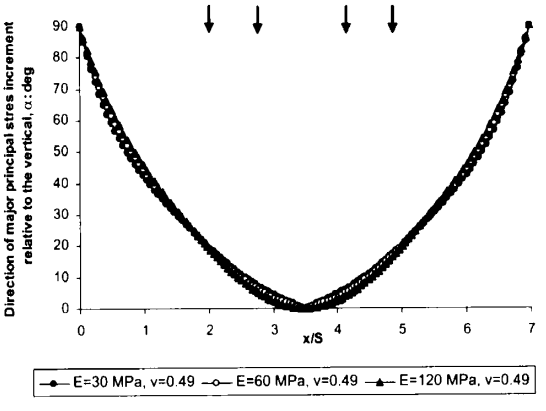


Fig. 11 The influence of wheel load location on vertical stress at different depths





**Fig. 12** Effect of stiffness on the rotation of the major principal stress increment direction: (a) at depth of 0.49S (C2 in Fig. 3); (b) at depth of 1.67S (C3 in Fig. 3)

At the shallower depth (0.49S), the major principal stress increment is (as would be expected) at or near vertical below the wheels and (due to Poisson's ratio effects) horizontal at the centres of the box wagons. Between the box wagons, the major principal stress increment remains near vertical in the analyses with  $E=30\,\mathrm{MPa}$  and  $E=60\,\mathrm{MPa}$ , but becomes horizontal when E is increased to 120 MPa. Apart from this, the curves shown in Fig. 12(a) for a depth of 0.49S are similar. At a depth of 1.67S, the results are practically independent of the stiffness used.

### 3.2 Effect of heterogeneity (stiffness increasing linearly with depth)

To investigate the effect of increasing stiffness with depth (heterogeneity), analyses were carried out with a Young's modulus that increased with depth from  $30\,\mathrm{MPa}$  at the surface at a rate of either  $10.89\cdot(z/S)\,\mathrm{MPa}$  or  $21.78\cdot(z/S)\,\mathrm{MPa}$ , i.e.  $E=30+10.89\cdot$ 

Proc. IMechE Vol. 221 Part F: J. Rail and Rapid Transit

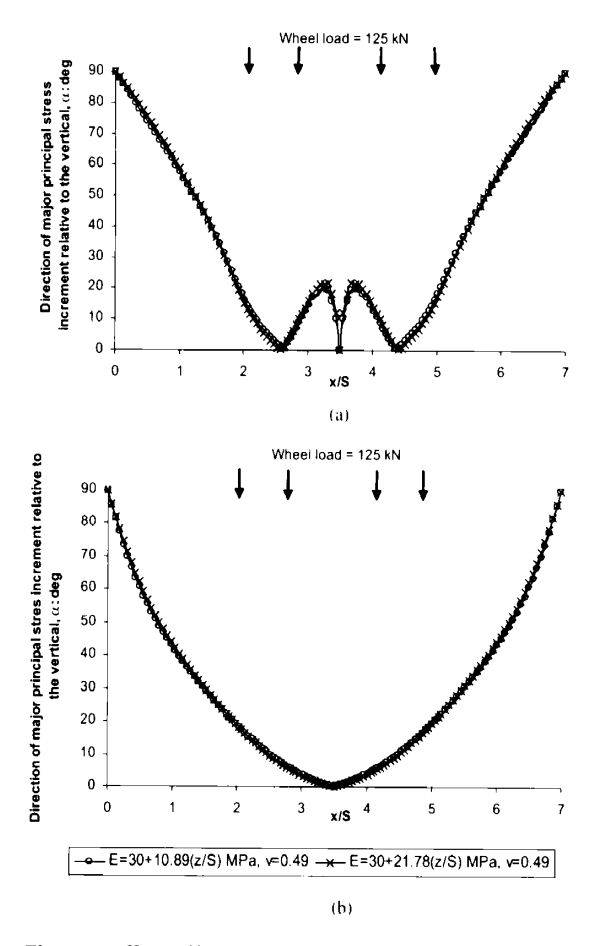


Fig. 13 Effect of heterogeneity (stiffness increasing linearly with depth) on the rotation of the major principal stress increment direction: (a) at depth of 0.49S (C2 in Fig. 3); (b) at depth of 1.67S (C3 in Fig. 3)

(z/S) MPa or  $E=30+21.78\cdot(z/S)$  MPa with Poisson's ratio  $\upsilon=\upsilon_{\rm u}\approx0.49$ , approximating constant volume conditions.

The results of these analyses are summarized in Fig. 13. There is no discernible difference at a depth of either 0.49S or 0.67S, and at both depths, the results are very similar to those for the homogeneous soil with  $E=30\,\mathrm{MPa}$ .

### 3.3 Effect of Poisson's ratio

Figure 14 shows the results of the analyses carried out for a Gibson soil with  $E=30+10.89\cdot(z/S)$  MPa undrained and Poisson's ratios  $\upsilon=0.49,~0.3,~$  and 0.1. The reduced Poisson's ratios could be viewed as modelling a partly saturated soil, in which volume changes could occur without any overall loss of pore water. In the analyses with the reduced Poisson's ratios  $\upsilon<0.49,~$  the Young's moduli were multiplied

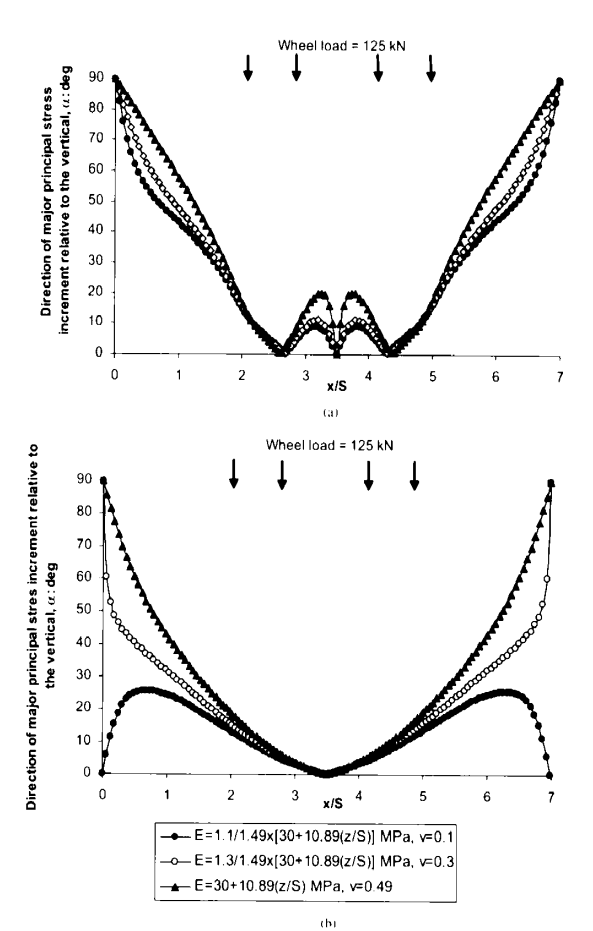


**Fig. 14** Effect of Poisson's ratio on the rotation of the major principal stress increment direction: (a) at depth of 0.49*S* (C2 in Fig. 3); (b) at depth of 1.67*S* (C3 in Fig. 3)

by  $(1+\nu)/(1.49)$  to maintain the equality of the shear modulus.

At a depth of 0.49S, decreasing the Poisson's ratio alters the rate at which the major principal stress increment turns towards the horizontal as the centres of the box cars are approached. At a depth of 1.67S, the differences between the various analyses apparent at 0.49S in between the box wagons are reduced, whereas those near the centres of the box wagons are amplified. Between the box wagons, the major principal stress increment remains vertical for all three values of Poisson's ratio. Near the centres of the box wagons, the major principal stress increment only just becomes horizontal when  $\upsilon=0.3$  and remains near vertical for the Gibson soil with  $\upsilon=0.1$ .

### 3.4 Effects of anisotropy

Many natural soils are deposited in horizontal layers and may be considered as being cross-anisotropic,

Proc. IMechE Vol. 221 Part F: J. Rail and Rapid Transit

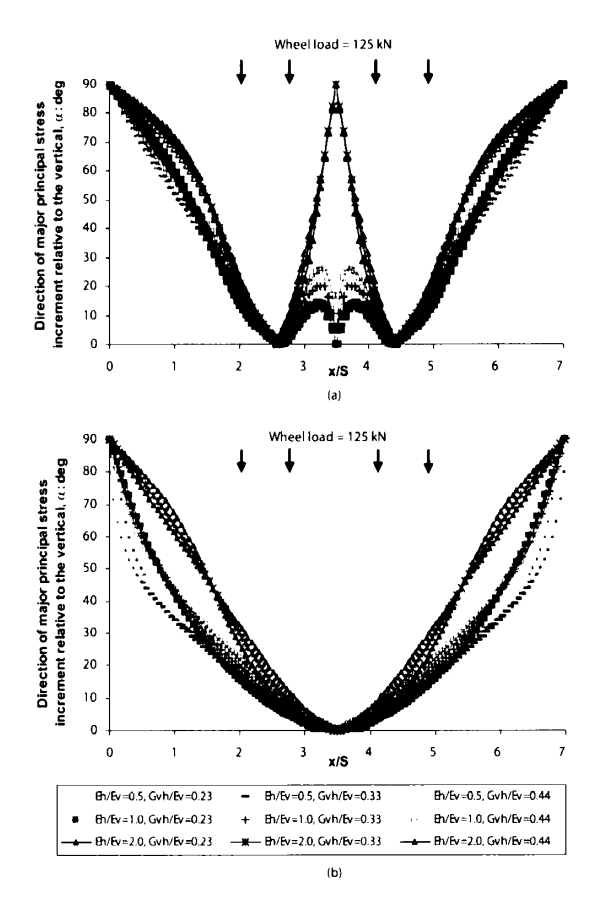


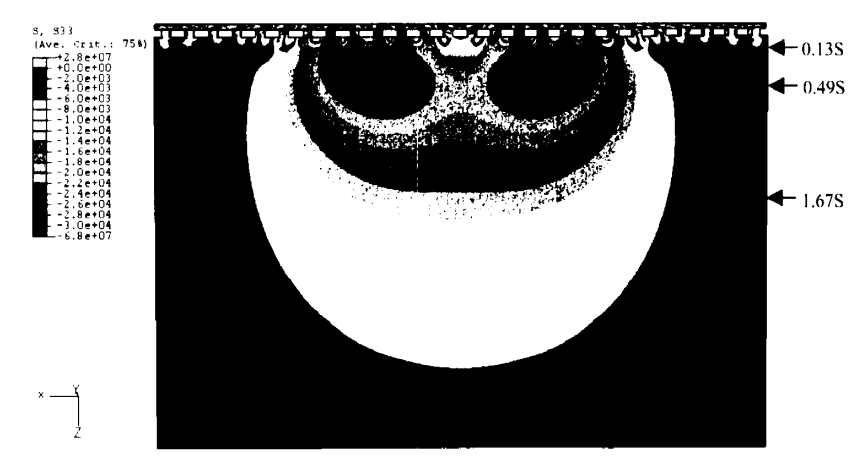
**Fig. 15** Effect of cross-anisotropy on the rotation of the major principal stress increment direction: (a) at depth of 0.49S (C2 in Fig. 3); (b) at depth of 1.67S (C3 in Fig. 3)

with elastic properties that are the same in both horizontal directions but different in the vertical [25]. The undrained (constant volume) elastic behaviour of such a material is governed by three independent parameters [21]:  $E_{\rm v}$ ,  $E_{\rm h}$ , and  $G_{\rm vh}$ , with deformation at constant volume requiring Poisson's ratios  $\upsilon_{\rm hh}=1-E_{\rm h}/2E_{\rm v}$ ,  $\upsilon_{\rm hv}=E_{\rm h}/2E_{\rm v}$ , and  $\upsilon_{\rm vh}=0.5$ . Lee and Rowe [25] give typical ranges of 0.5–2.4 for  $E_{\rm h}/E_{\rm v}$  and 0.2–0.4 for  $G_{\rm vh}/E_{\rm v}$ .

Nine analyses were carried out with the natural ground modelled as a Gibson soil, having  $E_{\rm v}=30+10.89\cdot(z/S)$  MPa,  $\nu_{\rm vh}=0.49$ ,  $E_{\rm h}/E_{\rm v}=0.5$ , 1, and 2, and  $G_{\rm vh}/E_{\rm v}=0.23$ , 0.33, and 0.44. The results of these analyses are shown in Fig. 15. Broadly, the results fall into three bands, governed by the ratio of the Young's moduli  $E_{\rm h}/E_{\rm v}$ . The effect of the ratio  $G_{\rm vh}/E_{\rm v}$  was of lesser importance, except perhaps for  $E_{\rm h}/E_{\rm v}=0.5$  and 1 between the bogies at a depth of 0.49S. At this location for  $E_{\rm h}/E_{\rm v}=2$ , the direction of the major principal stress increment returned to the horizontal.

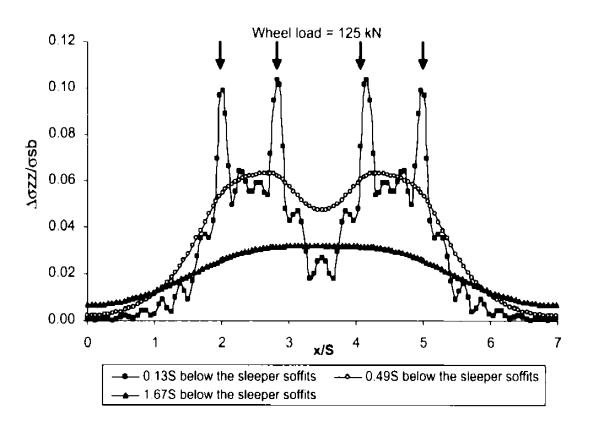
Figure 16 shows the contours of vertical stress increase due to wheel loading on the central longitudinal plane of the railway track. Figure 17 shows these vertical stress increases plotted against the distance from the centre-line of the first box wagon for depths of 0.13S, 0.49S, and 1.67S below the sleeper soffit. Both figures show quite clearly the transition with depth from axle loading (apparent at 0.13S) to bogie loading (at 0.49S) to wagon loading (at 1.67S). The magnitude of the maximum vertical stress increment decreases rapidly with depth, from 0.1 $\sigma_{sb}$  at a depth of 0.13S to 0.03 $\sigma_{sb}$  at a depth of 1.67S, due to the spreading of the loaded area.

Figure 18 shows the calculated changes in all six stress components ( $\sigma_{xx}$ ,  $\sigma_{yy}$ ,  $\sigma_{zz}$ ,  $\tau_{xy}$ ,  $\tau_{xz}$ , and  $\tau_{yz}$ ) at



**Fig. 16** Contours of vertical stress increment at the centre plane (compressive stress negative; three-dimensional FEA, with  $E=30+10.89\cdot(z/S)$  and  $\upsilon=0.49$  for the natural ground, without initial stresses)

Proc. IMechE Vol. 221 Part F: J. Rail and Rapid Transit



**Fig. 17** Variation in vertical stress increment on the centre plane with longitudinal distance, for different depths (3D FEA, with  $E=30+10.89\cdot(z/S)$  and  $\upsilon=0.49$  for the natural ground, without initial stresses)

depths of 0.13S, 0.49S, and 1.67S on the central longitudinal plane. In all cases, both the magnitude and the differentiation between individual axle loads decreases rapidly with depth. As would be expected, the variation in the shear stresses  $\tau_{xy}$  and  $\tau_{yz}$  was zero, so that the principal stress direction always remained in the xz plane. The variation of the inclination of the major principal stress increment to the vertical with distance from the centre of the first wagon is shown in Fig. 19.

Off the centre plane, changes in shear stress and hence PSR occurred in both vertical planes, as indicated in Fig. 20. However, the largest changes in shear stress were still in  $\tau_{xz}$ , with an amplitude of variation about twice as that of the shear stresses  $\tau_{xy}$  and  $\tau_{yz}$ .

### 3.5 Influence of initial stresses

The rotations in major principal stress direction reported above are for incremental loading. In reality, the absolute stress state and hence the amount and/or frequency of PSR will depend on the in situ stresses as well. This was investigated by superimposing the stresses caused by the passage of a train onto possible stress states in the natural ground, following construction of the raised sections of prepared subgrade, sub-ballast, ballast, and track but prior to train loading. Starting with a level ground surface with horizontal effective stresses given by an initial in situ earth pressure coefficient  $K_0 = \sigma'_{h0}/\sigma'_{v0}$  set to either 0.5, 1.0, or 2.0 (representing the likely range from normally consolidated to heavily overconsolidated conditions), the raised sections of prepared subgrade, sub-ballast. ballast, and track were constructed and their selfweight generated additional stresses in the natural ground prior to the application of the wheel loads.

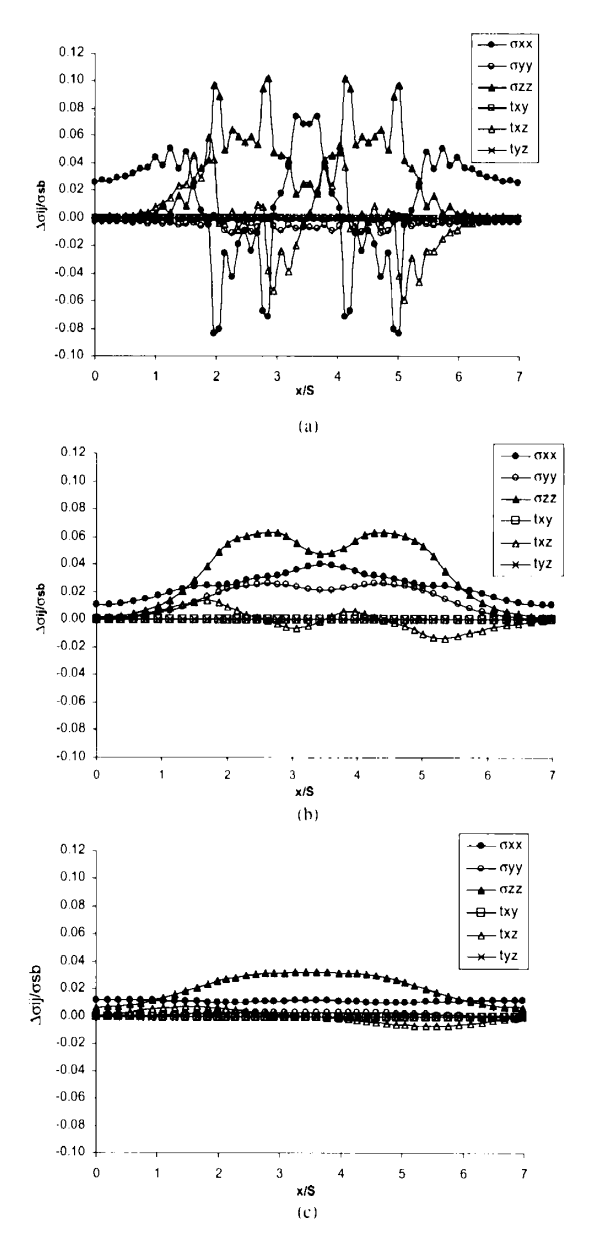


**Fig. 18** Variation in components of stress increment on the centre plane with longitudinal distance: (a) at depth of 0.13S (C1 in Fig. 3); (b) at depth of 0.49S (C2 in Fig. 3); (c) at depth of 1.67S (C3 in Fig. 3) (3D FEA, with  $E=30+10.89\cdot(z/S)$  and  $\upsilon=0.49$  for the natural ground, without initial stresses)

The PSRs on the central longitudinal plane obtained by superimposing the changes in stress due to train passage onto the post-construction *in situ* stresses are shown in Fig. 21.

The results at a depth of 0.13S below the sleeper soffit were unaffected by the *in situ* stress state,

Proc. IMechE Vol. 221 Part F: J. Rail and Rapid Transit

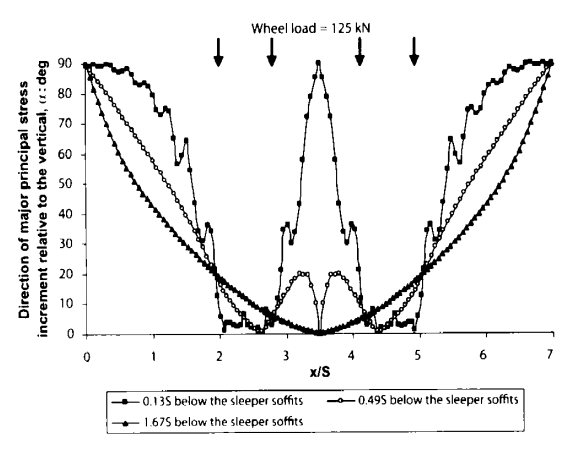


**Fig. 19** Variation of major principal stress increment direction with longitudinal distance at different depths on the centre plane (3D FEA, with  $E=30+10.89\cdot(z/S)$  and  $\upsilon=0.49$  for the natural ground, without initial stresses)

because this depth lies within the placed material zone at the top of the sub-ballast. At a depth of 0.49S, the variation in the orientation of the major principal stress is quite sensitive to the *in situ* stress state, varying from horizontal to vertical when  $K_0$  is greater than 1 but by only  $20^\circ$  or so from the vertical when  $K_0 = 0.5$ . With increasing depth, the *in situ* stresses increase and their influence on the direction of the major principal stress begins to dominate. By a depth of 1.67S, the major principal stress deviates from its initial orientation by  $<20^\circ$  for  $K_0 = 1$  and by  $<10^\circ$  for  $K_0 = 0.5$  and  $K_0 = 2$ .

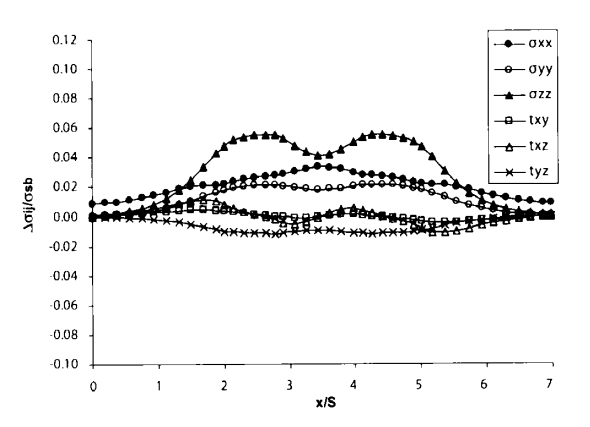


**Fig. 20** Variation in components of stress increment at a depth of 0.49S below the end of the sleeper (E in Fig. 3) (3D FEA, with  $E=30+10.89\cdot(z/S)$  and  $\upsilon=0.49$  for the natural ground, without initial stresses)

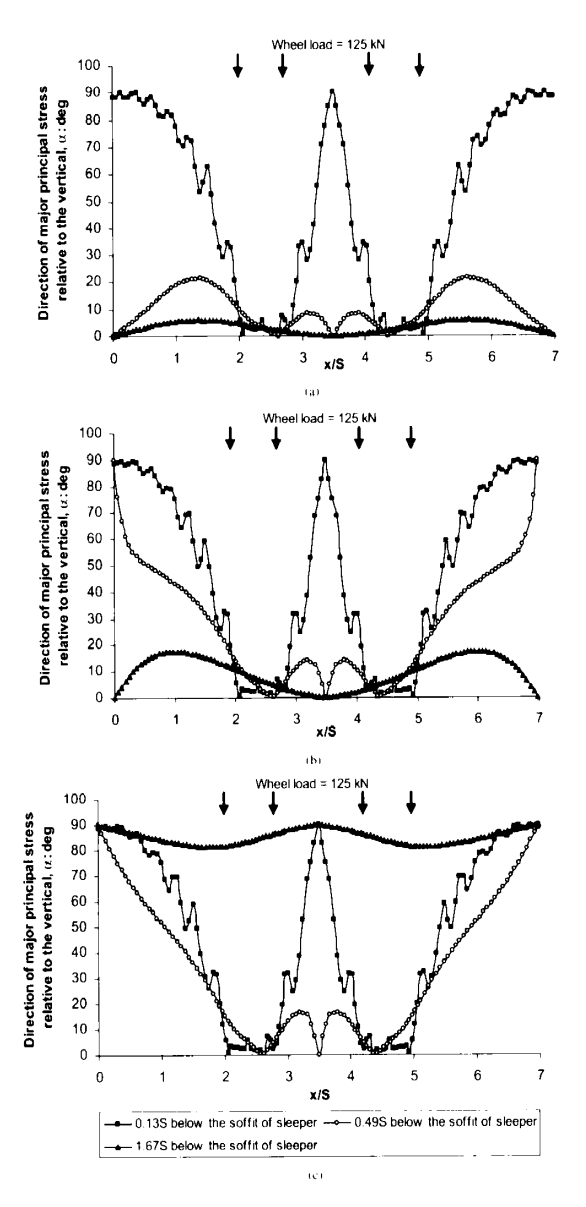


**Fig. 21** Variation in direction of major principal stress with longitudinal distance at different depths below the centre-line for different initial stress states (a)  $K_0 = 0.5$ ; (b)  $K_0 = 1.0$ ; (c)  $K_0 = 2.0$  (3D FEA, with  $E = 30 + 10.89 \cdot (z/S)$  and v = 0.49 for the natural ground, with initial stresses)

### 4 DISCUSSION IN THE CONTEXT OF LABORATORY ELEMENT TESTING USING THE HOLLOW CYLINDER APPARATUS

The numerical analyses have illustrated that the changes in stress to which an element of soil below a railway line are subjected as a train passes are complex. The magnitude and number of the stress cycles,

Proc. IMechE Vol. 221 Part F: J. Rail and Rapid Transit

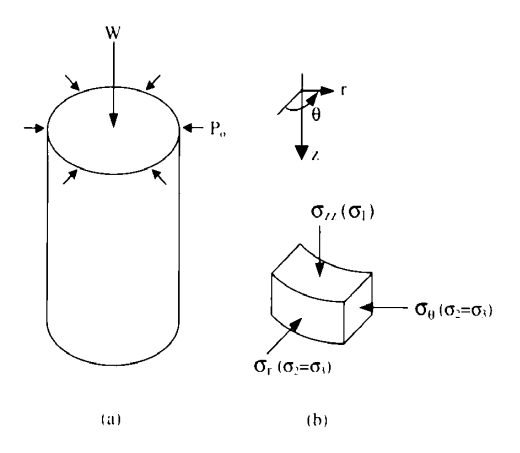


**Fig. 22** Stresses in a triaxial test subject to axial load, W and cell pressure,  $p_0$ : (a) triaxial sample; (b) stresses on an element

and whether they cause a marked change in the direction of the major principal stress, will depend on the depth and position of the soil element and its *in situ* stress state. The effect of these cyclic stress changes, which will also depend to some extent on the degree of anisotropy, can only be investigated by means of laboratory element tests.

In a conventional triaxial test, only the vertical stress  $\sigma_{zz}$  and the horizontal stress  $\sigma_{xx} = \sigma_{yy}$  (i.e.  $\sigma_{u} = \sigma_{r}$ ) can be controlled, and all of these are constrained to be principal stresses, i.e.  $\tau_{xy} = \tau_{xz} = \tau_{yz} = 0$  ( $\tau_{ur} = \tau_{uz} = \tau_{rz} = 0$ ) (Fig. 22). Thus, the complex pattern of stress changes experienced by railway track sub-bases cannot be approximated in this apparatus.

In the hollow cylinder apparatus (Fig. 23), the average vertical stress  $\sigma_{zz,av}$  can be controlled by means of the applied vertical load (W), the internal ( $p_i$ ), and external ( $p_o$ ) cell pressures

$$\sigma_{zz,av} = \frac{W}{\pi (r_o^2 - r_i^2)} + \frac{p_o \cdot r_o^2 - p_i \cdot r_i^2}{r_o^2 - r_i^2}$$
(3)

and the average shear stress applied to the horizontal plane,  $\tau_{zx,av}(\tau_{z'',av})$ , can be controlled by the applied torque  $(M_T)$ 

$$\tau_{zv,av} = \frac{3M_{\rm T}}{2\pi (r_{\rm o}^3 - r_{\rm i}^3)} \tag{4}$$

The average radial  $\sigma_{y,av}(\sigma_{r,av})$  and hoop  $\sigma_{x,av}(\sigma_{\theta,av})$  stresses can be controlled by means of the internal  $(p_i)$  and external  $(p_o)$  cell pressures

$$\sigma_{xx,av} = \frac{r_o \cdot p_o - r_i \cdot p_i}{r_o - r_i} \tag{5}$$

and

$$\sigma_{yy,av} = \frac{r_o \cdot p_o + r_i \cdot p_i}{r_o + r_i} \tag{6}$$

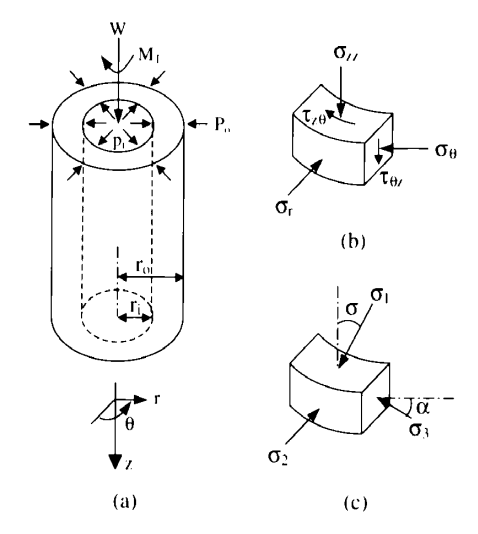


**Fig. 23** Idealized stress conditions in a hollow cylindrical element subject to axial load W, torque  $M_{\rm T}$ , internal pressure  $p_{\rm i}$ , and external pressure  $p_{\rm o}$ : (a) hollow cylinder sample; (b) stress on an element in the wall; (c) principal stress on an element in the wall (from reference [26])

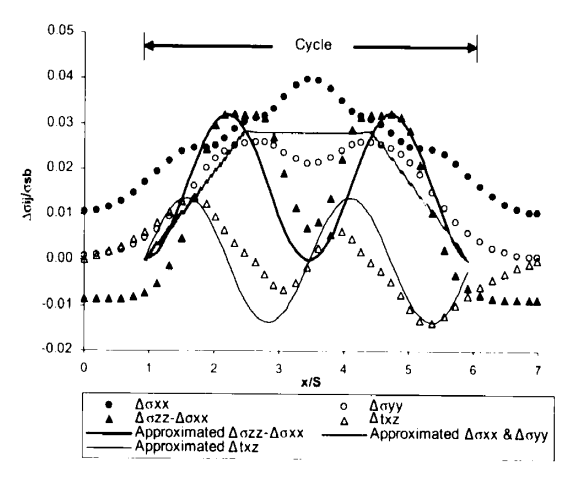


**Fig. 24** Approximate stress path for a soil element at the surface of natural ground (at depth of 0.49*S*), subject to train loading

where  $r_0$  is the outer radius and  $r_i$  the inner radius of the sample [26].  $\sigma_{xx,av}$  and  $\sigma_{yy,av}$  are equal if the same pressure acts inside and outside the cylinder, i.e. if  $p_0 = p_i$ .

Hence, it is possible to control the stress components  $\sigma_{zz,av}$ ,  $\sigma_{yy,av}$ ,  $\sigma_{xx,av}$ , and  $\tau_{zx}$ , although the shear stress components  $\tau_{xy}$  and  $\tau_{yz}$  are zero. This means that the stress paths experienced by soil elements on the central longitudinal plane below the track can easily be approximated in the cyclic hollow cylinder apparatus, as suggested by Brown [11]. Figure 24

shows how the stress paths illustrated in Fig. 18(b) at the surface of the natural ground (i.e. at a depth of 0.49S below the sleeper soffit) might be simulated. These would need to be superimposed on the estimated in situ stress state, after construction of the railway. Provided that  $E_{\rm h}/E_{\rm v}$  is not greater than 1 and that the soil may be characterized by means of a stiffness modulus that is not very large and is either constant or increases linearly with depth, these stress paths are not too sensitive to the elastic parameters.

Simulation of the out-of-plane PSRs experienced by soil elements off the centre plane can also be simulated using the hollow cylinder apparatus, provided that the vertical plane in which the principal stress rotates (which will be at an angle to the direction of the track when viewed in plan) is identified and used as the z- $\theta$  plane in the apparatus.

### 5 CONCLUSIONS

Two- and three-dimensional numerical analyses have been carried out to investigate the stresses experienced by soil elements in the natural ground below a railway track during train passage. The effects of the depth of the element, the initial *in situ* stress state of the soil, and the elastic parameters used to characterize the soil have been investigated. The analyses have shown the following.

- 1. Both the magnitude and the number of loading cycles during train passage reduce with depth. Stresses change in response to individual axle loads at depths <0.13S, to individual bogies at depths between 0.13S and 0.49S, and to pairs of bogies below a depth of 1.67S.
- 2. In an isotropic analysis at constant volume ( $\nu = \nu_u \approx 0.5$ ), the degree of principal stress increment rotation was not significantly affected at any depth by either the stiffness or the rate of increase of stiffness with depth, provided the stiffness was not too high (60 MPa or less). Variations in Poisson's ratio  $\nu$  between 0.3 and 0.49 were also not significant.
- 3. When the soil was modelled as a cross-anisotropic Gibson material, the variation in the direction of the major principal stress increment with the horizontal distance from the load depended more on the ratio  $E_{\rm h}/E_{\rm v}$  than on the ratio  $G_{\rm vh}/E_{\rm v}$ . Even so, the degree of principal stress increment rotation was not particularly sensitive to the elastic parameters provided that  $E_{\rm h}/E_{\rm v} \leqslant 1$ .
- 4. Along the centre of the track, the major and minor principal stresses remained in the vertical longitudinal plane because the shear stresses  $\tau_{xy}$  and  $\tau_{yz}$  were zero. Away from the centre plane, the changes

- in shear stress and hence PSR occurred in both vertical planes but the largest changes in shear stress were still in  $\tau_{xz}$ .
- 5. Rotation of the overall major principal stress is quite sensitive to the *in situ* stress state at a depth of 0.49*S*. With increasing depth, the *in situ* stresses increase and their influence begins to dominate; at a depth of 1.67*S*, the major principal stress does not deviate from its initial orientation by more than 20°. The effect of the initial stress state is easily taken into account in laboratory tests, by selecting appropriate starting conditions.
- 6. In the hollow cylinder apparatus, the initial *in situ* stress state could be modelled by the application of appropriate combinations of initial axial load, inner and outer cell pressures, and pore water pressure. Stress components induced by wheel loads below the centre-line of the track could then be modelled by superimposing the idealized sine or trapezoidal curves of suitable magnitude. Simulation of the out-of-plane PSRs experienced by soil elements off the centre plane requires identification of the principal plane, which will lie at an angle to the direction of the track when viewed in plan.

#### **ACKNOWLEDGEMENTS**

The work described in this article was carried out under the auspices of Rail Research UK and financed by grants from the Engineering and Physical Sciences Research Council (grant no. GR/S12784/01). The analyses were inspired by Dr Daren Bowness, whose untimely death in July 2005 deprived us of a valued friend and a respected colleague.

#### REFERENCES

- 1 American Railway Engineering Association (AREA).

  Manual for railway engineering, 1996, vol. 1 (AREA, Washington, DC).
- 2 Raymond, G. P. Design for railroad ballast and subgrade support. *J. Geotech. Eng. Div., Proc. Am. Soc. Civil Eng.* (ASCE), 1978, 104(GT1), 45–60.
- 3 Selig, E. T. and Waters, J. W. *Track geotechnology* and substructure management, 1994 (Thomas Telford, London, UK).
- 4 Casagrande, A. Classification and identification of soils. Proc. Am. Soc. Civil Eng. (ASCE), 1947, 73(6), 783–810.
- 5 Heath, D. L., Shenton, M. J., Sparrow, R. W., and Waters, J. M. Design of conventional rail track foundations. Proc. Inst. Civ. Eng., Part 1, 1972, 51(2), 251–267.
- **6 Li, D.** and **Selig, E. T.** Method for railroad track foundation design I: applications. *J. Geotech. Geoenviron. Eng.*, 1998, **124**(4), 316–322.

Proc. IMechE Vol. 221 Part F: J. Rail and Rapid Transit

- 7 Li, D. and Selig, E. T. Method for railroad track foundation design II: development. J. Geotech. Geoenviron. Eng., 1998, 124(4), 323–329.
- **8 Li, D.** and **Selig, E. T.** Cumulative plastic deformation for fine-grained subgrade soils. *J. Geotech. Eng.*, 1996, **122**(12), 1006–1013.
- 9 Suiker, S. J., Selig, E. T., and Frenkel, R. Static and cyclic triaxial testing of ballast and subballast. *J. Geotech. Geoenviron. Eng.*, 2005, 131(6), 771–782.
- 10 American Association of State Highway and Transportation Officials (AASHTO). Standard method of test for resilient modulus of subgrade soils, 1986 (AASHTO Designation T272-82, Washington, DC).
- 11 Brown, S. F. Soil mechanics in pavement engineering. Geotechnique, 1996, 46(3), 384–426.
- 12 Grabe, P. J. Resilient and permanent deformation of railway foundations under principal stress rotation. PhD Dissertation. University of Southampton, UK, 2002.
- 13 Grabe, P. J., Clayton, C. R. I., and Shaw, F. J. Deformation measurement on a heavy haul track formation. In Proceedings of the 8th International Heavy Haul Conference, Rio de Janeiro, Brazil, 2005, pp. 287–295.
- **14 Hibbitt, Karlsson & Sorensen, Inc.** *ABAQUS/standard user's manuals, version* 6.5, 2005 (Hibbitt, Karlsson & Sorensen, Inc. Pawtucket, RI).
- 15 The Permanent Way Institution (PWI). British Railway track design, construction and maintenance, 6th edition (Ed. G. H. Cope), 1993 (Echo Press, Loughborough, Leicester, UK).
- **16 International Union of Railways (UIC).** *UIC Code 719R: Earthworks and trackbed layers for railway lines*, 1994 (UIC, Paris, France).
- 17 O'Riordan, N. and Phear, A. Design and construction of ballasted track formation and subgrade for high speed lines. In Proceedings of the International Conference of Railway Engineering, 2001, London.
- **18 Esveld, C.** *Modern railway track*, 2001 (MRT-Productions, Zaltbommel, The Netherlands).
- 19 Oberg, E., Jones, F. D., Horton, H. L., and Ryffel, H. H. Machinery's handbook (Eds C. J. McCauley, R. M. Heald, and M. I. Hussain), 27th edition, 2004 (Industrial Press, New York)
- 20 Kaynia, A. M., Madshus, C., and Zackrisson P. Ground vibration from high-speed trains: prediction and countermeasure. J. Geotech. Geoenviron. Eng., 2000, 126(6), 531–537.
- **21 Gibson, R. E.** The analytical method in soil mechanics. *Geotechnique*, 1974, **24**(2), 115–140.
- 22 Burland, J. B. and Kalra, J. C. Queen Elizabeth Il Conference Centre: geotechnical aspects. *Proc. Inst. Civ. Eng.*, *Part 1*, 1986, **80**, 1479–1503.
- 23 Poulos, H. G. and Davis, E. H. Elastic solutions for soil and rock mechanics, 1974 (New York, Wiley).
- 24 Burland, J. B., Broms, B., and de Mello, V. F. B. Behaviour of foundations and structures: state-of-art review. In Proceedings of Ninth International Conference on Soil Mechanics and Foundation Engineering, Tokyo, 1977, vol. 2, pp. 495–546.

- **25 Lee, K. M.** and **Rowe, R. K.** Deformations caused by surface loading and tunnelling: the role of elastic anisotropy. *Geotechnique*, 1989, **39**(1), 125–140.
- 26 Hight, D. W., Gens, A., and Symes, M. J. The development of a new hollow cylinder apparatus for investigating the effects of principal stress rotation in soils. *Geotechnique*, 1983, 33(4), 355–383.

### **APPENDIX**

#### Notation

Notation	
а	sleeper spacing
av	subscribe for average values
Ε	Young's modulus
$E_{\mathrm{h}}$	Young's modulus in the horizontal
	direction
$E_{\rm v}$	Young's modulus in the vertical direc-
	tion
$E_0$	Young's modulus at the ground surface
G	shear modulus
$G_{ m vh}$	shear modulus in $v$ - $h$ plane
h	depth of the natural ground layer
	(mesh size in the two-dimensional
	FEA)
I	moment of inertia
$K_0$	lateral earth pressure coefficient at rest
m	Young's modulus gradient as a function
	of depth
$M_{\mathrm{T}}$	applied torque in the hollow cylinder
	apparatus
$p_{\mathrm{i.}}p_{\mathrm{o}}$	internal and external cell pressures,
	respectively, for the hollow cylinder
	apparatus
$r_0, r_1$	outer and inner rad, respectively, of a
0	hollow cylinder sample
S	sleeper length
W	sleeper width
W	applied vertical load
x	longitudinal direction transverse direction
y	vertical direction
Z	vertical direction
α	the direction of the major principal
	stress, relative to the vertical
Δ	prefix denoting increment (usually of
	stress)
v	Poisson's ratio
v'	Poisson's ratio (effective stresses)
$v_{\mathfrak{u}}$	Poisson's ratio for undrained (constant
	volume) deformation of an isotropic
	material Control of the control of t
$v_{ m hh}$	Poisson's ratio for the effect of horizon-
	tal stress on complementary horizontal
	strain

Poisson's ratio for the effect of horizon-

tal stress on vertical strain

 $v_{\mathrm{hv}}$ 

$v_{ m vh}$	Poisson's ratio for the effect of	$\sigma_{ m sb}$	notional maximum surface stress
	vertical stress on horizontal strain		(an axle load divided by the
$\rho$	maximum ground surface dis-		sleeper area)
	placement	$\sigma_{ m h0}^{\prime}$	initial effective horizontal stress
$\sigma_{\rm r}$ , $\sigma_{\rm r}$	radial stress and tangential stress	$\sigma_{\mathrm{v0}}^{\prime\prime\prime}$	initial effective vertical stress
$\sigma_{xx}$ , $\sigma_{yy}$ , $\sigma_{zz}$	normal stresses in the $x$ , $y$ , and $z$	$ au_{nr},  au_{nz},  au_{rz}$	shear stresses in the $\theta r$ , $\theta z$ , and $rz$
	directions, respectively		planes, respectively,
$\sigma_1, \sigma_2, \sigma_3$	major, intermediate, and minor	$\tau_{xy}$ , $\tau_{xz}$ , $\tau_{yz}$	shear stresses in the xy, xz, and yz
	principal stresses, respectively		planes, respectively,